The Astrophysical Journal, 653:345–360, 2006 December 10

VARIATIONS IN THE D/H RATIO OF EXTENDED SIGHT LINES FROM *FAR ULTRAVIOLET SPECTROSCOPIC EXPLORER* OBSERVATIONS[1]

Cristina M. Oliveira[2] and Guillaume Hébrard[3]

Received 2006 July 28; accepted 2006 August 22

ABSTRACT

We use new *FUSE* data to determine the column densities of interstellar D I, N I, O I, Fe II, and H_2 along the HD 41161 and HD 53975 sight lines. Together with N(H I) from the literature, we derive D/H, N/H, and O/H ratios. These sight lines have $\log N(\mathrm{H\ I}) > 21.00$ and probe gas up to ~1300 pc, allowing us to determine the gas-phase D/H ratio in a hydrogen column density range, $\log N(\mathrm{H}) > 20.70$, where the only five measurements available in the literature yield a weighted average of $\mathrm{D/H} = (0.86 \pm 0.08) \times 10^{-5}$. We find $\mathrm{D/H} = (2.14^{+0.51}_{-0.43}) \times 10^{-5}$ along the HD 41161 sight line. This ratio is ~3 σ higher than the weighted mean D/H ratio quoted above, while the D/H ratio for the HD 53975 line of sight, $\mathrm{D/H} = (1.02^{+0.23}_{-0.20}) \times 10^{-5}$, agrees within the 1 σ uncertainties. Our D/H measurement along the HD 41161 sight line presents the first evidence of variations of D/H at high N(H). Our result seems to indicate either that the long sight lines that, according to the deuterium depletion model, are dominated by cold undisturbed gas where deuterium would be depleted onto carbonaceous grains occur at higher N(H) than previously thought, or that the clumping of low D/H values in the literature for the long sight lines has another explanation. Both of the O/H ratios derived here, $(9.12^{+2.15}_{-1.83}) \times 10^{-4}$ and $(5.37^{+1.35}_{-1.14}) \times 10^{-4}$ (for HD 41161 and HD 53975, respectively), are higher than what has been found by other authors. Finally, we derive $(N/\mathrm{H}) \times 10^5 = 8.32^{+2.09}_{-1.76}$ and $5.07^{+1.45}_{-1.21}$, and $(\mathrm{D/O}) \times 10^2 = 2.29^{+0.40}_{-0.35}$ and $1.91^{+0.51}_{-0.43}$, for HD 41161 and HD 53975, respectively. In addition, the relatively high signal-to-noise ratio of the HD 41161 data allows us to place constraints on the f-values of some neutral chlorine transitions present in the *FUSE* bandpass for which only theoretical values are available.

Subject headings: ISM: abundances — ISM: evolution — stars: individual (HD 41161, HD 53975) — ultraviolet: ISM

1. INTRODUCTION

Deuterium is thought to have been produced in appreciable amounts only in the big bang (Epstein et al. 1976). Of all the light elements produced during big bang nucleosynthesis (e.g., ^{3}He, ^{4}He, ^{7}Li), deuterium, easily destroyed in stellar interiors (astration), is the one whose relatively simple evolution makes it a particularly sensitive estimator of the baryonic density. Conversely, measurements of the cosmic microwave background, such as those performed with The *Wilkinson Microwave Anisotropy Probe* (*WMAP*) and other missions, can be used to infer the primordial abundance of deuterium, $(\mathrm{D/H})_P$. Analysis of the three year *WMAP* data (Spergel et al. 2006) yields $(\mathrm{D/H})_P$ in agreement with that derived by Kirkman et al. (2003), $(\mathrm{D/H})_P = (2.78^{+0.44}_{-0.38} \times 10^{-5})$, by taking the weighted average of five D/H measurements toward quasi-stellar objects (QSOs) in the range $z = 2.079$–3.572. Sembach et al. (2004) found $\mathrm{D/H} = (2.2 \pm 0.7) \times 10^{-5}$ for Complex C, a high-velocity low-metallicity cloud falling into our Galaxy, which has presumably experienced more stellar processing than the gas seen toward QSOs.

Precise measurements of the gas-phase D/H ratio in the interstellar medium (ISM) were first performed with the *Copernicus* satellite (e.g., Rogerson & York 1973), followed by the *Hubble Space Telescope* 20 years later (*HST*; e.g., Linsky et al. 1995), IMAPS (Interstellar Medium Absorption Profile Spectrograph; Jenkins et al. 1999; Sonneborn et al. 2000), and more recently the *Far Ultraviolet Spectroscopic Explorer* (*FUSE*; e.g., Oliveira et al. 2006 and references therein). Variations in the D/H ratio were observed early on (York 1983), and by different satellites (e.g., Jenkins et al. 1999). Lemoine et al. (1999) discuss some of the mechanisms that could be responsible for the observed variations, based on the D/H data available at the time. However, only after the launch of *FUSE* in 1999 has a large enough sample of sight lines with differing D/H ratios been accumulated, allowing the question of what causes the D/H variations to be addressed in a more systematic way. While the constancy of the D/H ratio in the Local Bubble [LB; corresponding to $\log N(\mathrm{H}) \leq 19.2$; Sfeir et al. 1999] seems to be a well-accepted fact [$(\mathrm{D/H})_{\mathrm{LB}} = (1.56 \pm 0.04) \times 10^{-5}$ from the compilation by Wood et al. 2004] two distinct explanations have emerged to explain the large scatter of gas-phase D/H measurements in the solar neighborhood outside of the LB. These measurements range from $\mathrm{D/H} = (0.50 \pm 0.16) \times 10^{-5}$ toward θ Car, derived by Allen et al. (1992), to $\mathrm{D/H} = (2.18^{+0.22}_{-0.19}) \times 10^{-5}$ toward γ^2 Vel, derived by Sonneborn et al. (2000).

Hébrard & Moos (2003) proposed a low value for the present-epoch deuterium abundance in the solar neighborhood, based on indirect measurements of D/H from D/O and the constancy of the O/H ratio [$\mathrm{O/H} = (3.43 \pm 0.15) \times 10^{-4}$ from Meyer et al. (1998) updated f-value]. Using more measurements than Hébrard & Moos (2003), Hébrard (2006) proposed then $\mathrm{D/H} = (0.7 \pm 0.2) \times 10^{-5}$ for the present-epoch deuterium abundance. The high D/H ratios observed would be due to unknown systematic errors in the determination of N(H I), unknown deuterium enrichment processes, and/or local infall of deuterium-rich gas.

The possibility that deuterium could be depleted in dust grains was first proposed by Jura (1982). Draine (2004, 2006) explored further the theoretical plausibility of this process, leading Wood et al. (2004) and Linsky et al. (2006) to propose that the depletion of deuterium into dust grains leads to different levels of depletion

[1] Based on observations made with the NASA-CNES-CSA *Far Ultraviolet Spectroscopic Explorer*. *FUSE* is operated for NASA by the Johns Hopkins University under NASA contract NAS5-32985.

[2] Department of Physics and Astronomy, The Johns Hopkins University, 3400 North Charles Street, Baltimore, MD 21218.

[3] Institut d'Astrophysique de Paris, 98 bis, Boulevard Arago, 75014 Paris, France.

TABLE 1
STELLAR PROPERTIES

Star	d (pc)	l (deg)	b (deg)	Spectral Type	$v_{\sin i}$ (km s^{-1})	E_{B-V}
HD 41161.....	1253	164.97	+12.89	O8.0 V	300	0.20
HD 53975	1318	225.68	−2.32	O7.5 V	163	0.22

NOTES.—All stellar properties are from Diplas & Savage (1994a), except for the $v_{\sin i}$ values, which are from Howarth et al. (1997). Distances are based on photometry and are probably accurate within ∼25%.

along sight lines with different histories, producing the observed scatter in D/H. In this scenario, the highest measurements of the gas-phase abundance of deuterium in the solar neighborhood place a lower limit on the total deuterium abundance, $\mathrm{D/H} \geq (2.31 \pm 0.24) \times 10^{-5}$, which one can then compare to the primordial value through chemical evolution models. Supporting evidence for this model includes correlations of D/H with the depletion of Ti (Prochaska et al. 2005), Fe, and Si (Linsky et al. 2006), and with the average sight line density (Oliveira et al. 2006).

Galactic evolution models have to reproduce a number of observables, such as the metallicity distribution of late-type stars, along with predictions of the evolution of deuterium from its primordial value to its present-day distribution in the Galaxy, and in particular its value in the solar neighborhood. Romano et al. (2006) have addressed the different views on the behavior of the D/H ratio by considering what value of D/H is predicted for the solar neighborhood by chemical evolution models that satisfy the majority of the observational constraints (such as the G dwarf metallicity distribution). They find that a modest star formation and a continuous infall of unprocessed gas is required to fit all the observational data, leading only to a modest decrease of the deuterium abundance from its primordial value. According to the models of Romano et al. (2006), which adopt $(\mathrm{D/H})_P = 2.6 \times 10^{-5}$, D/H in the solar neighborhood should be in the range of $(1.4\text{–}2.0) \times 10^{-5}$, implying astration factors <1.8. Low D/H ratios, such as the one proposed by Hébrard (2006), are ruled out because they produce significant disagreements with other observational constraints, in particular with the G dwarf metallicity distribution.

Testing the two explanations above for the scatter in D/H requires more measurements of D/H and other species that might yield information about the depletion and physical conditions along the sight lines, particularly along high column density sight lines. In this work we present analyses of the D/H and other ratios along the extended sight lines to HD 41161 and HD 53975. Both of these sight lines have total hydrogen column densities greater than 10^{21} cm^{-2}, and according to the variable deuterium depletion model such high column density sight lines should be biased by cold, not recently shocked gas, where deuterium would be depleted in grains. For the HD 53975 sight line we find $\mathrm{D/H} = (1.02^{+0.23}_{-0.20}) \times 10^{-5}$, a value slightly higher than but comparable to those found previously for similar sight lines. The high D/H ratio along the HD 41161 sight line, $\mathrm{D/H} = (2.14^{+0.51}_{-0.43}) \times 10^{-5}$, presents the first evidence of D/H variations at high $N(\mathrm{H})$, indicating that our understanding of the behavior of D/H is still incomplete.

This paper is organized as follows. The targets and their sight lines are presented in § 2. Section 3 describes the observations and data processing, while § 4 presents the analyses. The abundance of neutral hydrogen along the two sight lines is discussed in § 5. The results are presented and discussed in § 6. Constraints on the f-values of Cl I transitions present in the spectra of HD 41161 are derived in § 7. Our work is summarized in § 8. All uncertainties are quoted at the 1 σ level unless noted otherwise.

2. THE TARGETS AND THEIR SIGHT LINES

The properties of the two stars are listed in Table 1. Below we discuss each star in detail.

2.1. *HD 41161*

HD 41161 (O8 V; Conti & Alschuler 1971) is a field star (Maíz-Apellániz et al. 2004) that probes gas in the direction $l = 164.^{\circ}97$ and $b = +12.^{\circ}89$ up to 1253 pc. Jenkins (1978) used *Copernicus* data to derive $\log N(\mathrm{O\ VI}) = 13.29$. Using *IUE* data, Shull & van Steenberg (1985) derived $\log N(\mathrm{H\ I}) = 20.98 \pm 0.07$, while Diplas & Savage (1994a) determined $\log N(\mathrm{H\ I}) = 21.01 \pm 0.08$, also from *IUE* data. Taking into account these two determinations of $N(\mathrm{H\ I})$, we adopt for the purpose of this study $\log N(\mathrm{H\ I}) = 21.00 \pm 0.09$.

Dixon et al. (1998) determined the column densities of H_2 ($J = 0\text{–}5$) along this sight line using *ORFEUS-1* data. The higher resolution and signal-to-noise ratio (S/N) of the *FUSE* data for HD 41161 allow us to determine H_2 column densities with uncertainties smaller than the ∼60% (or more) quoted by Dixon et al. (1998).

2.2. *HD 53975*

HD 53975 (O7.5 V; Conti & Alschuler 1971) is a spectroscopic binary (Garmany et al. 1980; Gies et al. 1994) member of the CMa OB1 association (Humphreys 1978), probing gas up to a distance of 1318 pc in the direction $l = 225.^{\circ}68$ and $b = -2.^{\circ}32$. Based on observations obtained with *Copernicus*, Bohlin et al. (1978) determined $\log N(\mathrm{H\ I}) = 21.15^{+0.08}_{-0.10}$. Shull & van Steenberg (1985) used *IUE* data to derive $\log N(\mathrm{H\ I}) = 21.11 \pm 0.08$, while Diplas & Savage (1994a) determined $\log N(\mathrm{H\ I}) = 21.10 \pm 0.08$, also from *IUE* data. We take the weighted average of the independent $N(\mathrm{H\ I})$ determinations based on *Copernicus* and *IUE* (Shull & van Steenberg 1985) data to adopt for this work $\log N(\mathrm{H\ I}) = 21.13 \pm 0.06$.

3. OBSERVATIONS AND DATA PROCESSING

The *FUSE* observatory consists of four coaligned prime-focus telescopes and Rowland-circle spectrographs that produce spectra over the wavelength range 905–1187 Å, with a spectral resolution of ∼15–20 km s^{-1} (wavelength dependent) for point sources. Two of the optical channels employ SiC coatings, providing reflectivity in the wavelength range ∼905–1000 Å, while the other two have LiF coatings for maximum sensitivity above 1000 Å. Dispersed light is focused onto two photon-counting microchannel plate detectors. With this arrangement of optical channels (LiF 1, LiF 2, SiC 1, and SiC 2) and detector segments (1A, 1B, 2A, and 2B), the *FUSE* instrument has eight channels:

TABLE 2
Log of *FUSE* Observations

Star	Program ID	Aperture	Mode	Time (s)	Date	CalFUSE
HD 41161.....	P1021001	LWRS	HIST	58	2001 Feb 20	3.0.7
	P1021002[a]	MDRS	HIST	6520	2003 Sep 25	3.0.8
HD 53975	P3032301[a]	MDRS	HIST	482	2004 Feb 04	3.0.7

[a] Only SiC data obtained during these observations.

LiF 1A, LiF 1B, LiF 2A, LiF 2B, SiC 1A, SiC 1B, SiC 2A, and SiC 2B. Four channels cover the wavelength range 1000–1080 Å, while two channels each cover the ranges 900–1000 and 1080–1180 Å. Details about the *FUSE* mission, its planning, and on-orbit performance can be found in Moos et al. (2000) and Sahnow et al. (2000).

Table 2 summarizes the *FUSE* observations of HD 41161 and HD 53975. HD 41161 was observed by *FUSE* through the large (LWRS; $30'' \times 30''$) and medium-sized (MDRS; $4'' \times 20''$) apertures. During the short (58 s) LWRS observation data were obtained with the LiF and SiC channels. During the longer (6520 s) MDRS observation only SiC data were obtained due to the flux of this star being very close to the *FUSE* bright-object limit (10^{-10} ergs s^{-1} Å^{-1} cm^{-2}). The lower reflectivity of the SiC channels compared to that of the LiF channels allows some bright targets to be observed without damaging effects on the detectors.

The two-dimensional *FUSE* spectra are reduced using the CalFUSE pipeline, version 3.[4] The processing includes data screening for low-quality or unreliable data, thermal drift correction, geometric distortion correction, heliocentric velocity correction, dead-time correction, wavelength calibration, detection and removal of event bursts, background subtraction, and astigmatism correction. The spectra are aligned by cross-correlating the individual exposures over a short wavelength range that contains prominent spectral features, and then co-added by weighting each exposure by its exposure time, using the CORRCAL software developed by S. Friedman.

The S/N of the LWRS data obtained for the HD 41161 sight line is inferior to that of the MDRS data. In our analysis we use SiC data from the MDRS observation (no LiF data was obtained during this observation) and only LiF data from the LWRS observation. The coadded MDRS data has a S/N per pixel of 16.87 at ~918.5 Å in the SiC 1B channel and of 32.7 at ~1032.2 Å in the SiC 1A channel.

HD 53975 was observed by *FUSE* for 482 s through the MDRS aperture. Similarly to HD 41161, only SiC data were obtained during this observation due to the flux of this star being close to the *FUSE* bright-object limit. We coadded the data for this target in the manner described above. The co-added data have a S/N per pixel of 10.25 at ~918.5 Å in the SiC 1B channel and 16.87 at ~1032.6 Å in the SiC 1A channel.

Figures 1 and 2 present the *FUSE* spectra of the two targets.

4. ANALYSIS

We use apparent optical depth, curve of growth, and profile fitting methods (AOD, COG, and PF, respectively) to determine column densities along the sight lines whenever possible (see, e.g., Oliveira et al. [2003, 2006] for further discussion of these methods). Details about the particular fitting routine used here (Owens.f) can be found in Hébrard et al. (2002) and Lemoine et al. (2002).

Table 3 lists the atomic data and equivalent widths of the transitions used in this study. A, C, and P are used to indicate which transitions are used with the AOD, COG, and PF techniques, respectively. No equivalent widths were measured for the transitions flagged only with "P" due to blendings, or in the case of D I, because there are not enough unblended D I transitions to construct a curve of growth. These transitions were only used with the PF technique. We use the compilation by Morton (2003) for the atomic data and that of Abgrall et al. (1993a, 1993b) for the molecular data.

4.1. *Atomic Species along the Line of Sight to HD 41161*

We use the AOD technique to place lower limits on the column densities of C I, C III, N II, P II, Cl II, and Ar I along this sight line and to determine the column densities of D I, N I, and Fe II. With the COG method we derive column densities for N I and Fe II, and $b_{\rm N\,I} = 8.3 \pm 0.2$ km s^{-1} and $b_{\rm Fe\,II} = 9.2^{+1.0}_{-0.9}$ km s^{-1}.

The PF technique is used in a similar manner in the analyses of both sight lines. We fit a single absorption component to the low-ionization atomic species D I, N I, O I, and Fe II, and another to the molecular species. H I is included in the fit as well, in a separate absorption component, with the sole purpose of modeling the continuum in the vicinity of the D I lines. We use a line-spread function (LSF) with a FWHM of 0.0641 Å to fit the *FUSE* data, constant for all channels and wavelengths, corresponding to a spectral resolution of ~20 km s^{-1} (see Williger et al. [2005] for a determination of the LSF across the *FUSE* bandpass and for a comparison between N obtained with both free and fixed LSFs). We derive a Doppler parameter $b \sim 10$ km s^{-1} for the absorption component containing D I, N I, O I, and Fe II, in agreement with b derived for N I and Fe II with the COG technique. This Doppler parameter should not be viewed as the classic b composed of turbulent and thermal terms, but rather as the result of line broadening due to multiple unresolved components along the sight line. Fits to some of the lines used with the PF method are presented in Figure 3. N(D I) along this sight line is constrained mostly by the λ916.2 D I transition, which is free from blends with other lines, making N(D I) independent of $N(H_2)$.

Table 4 presents the column densities of the atomic species obtained with the different methods, as well as the adopted values. In this work we adopt values that are roughly at the midpoint of the values obtained with the different methods and uncertainties that include the extremes of the values obtained with the different methods. As a general rule we do not adopt 1 σ uncertainties smaller than 0.05 dex (~12%), because we feel that adopting smaller uncertainties could be misleading, due to the presence of unknown systematic effects.

O VI is not clearly detected in our data. Using the λ1032 O VI transition, we place a 3 σ upper limit on log N(O VI) of 13.0, while Jenkins (1978) determined log N(O VI) = 13.29 using *Copernicus* data. Since no uncertainties were quoted by Jenkins (1978), and

[4] The CalFUSE pipeline reference guide is available at http://fuse.pha.jhu.edu/analysis/pipeline_reference.html.

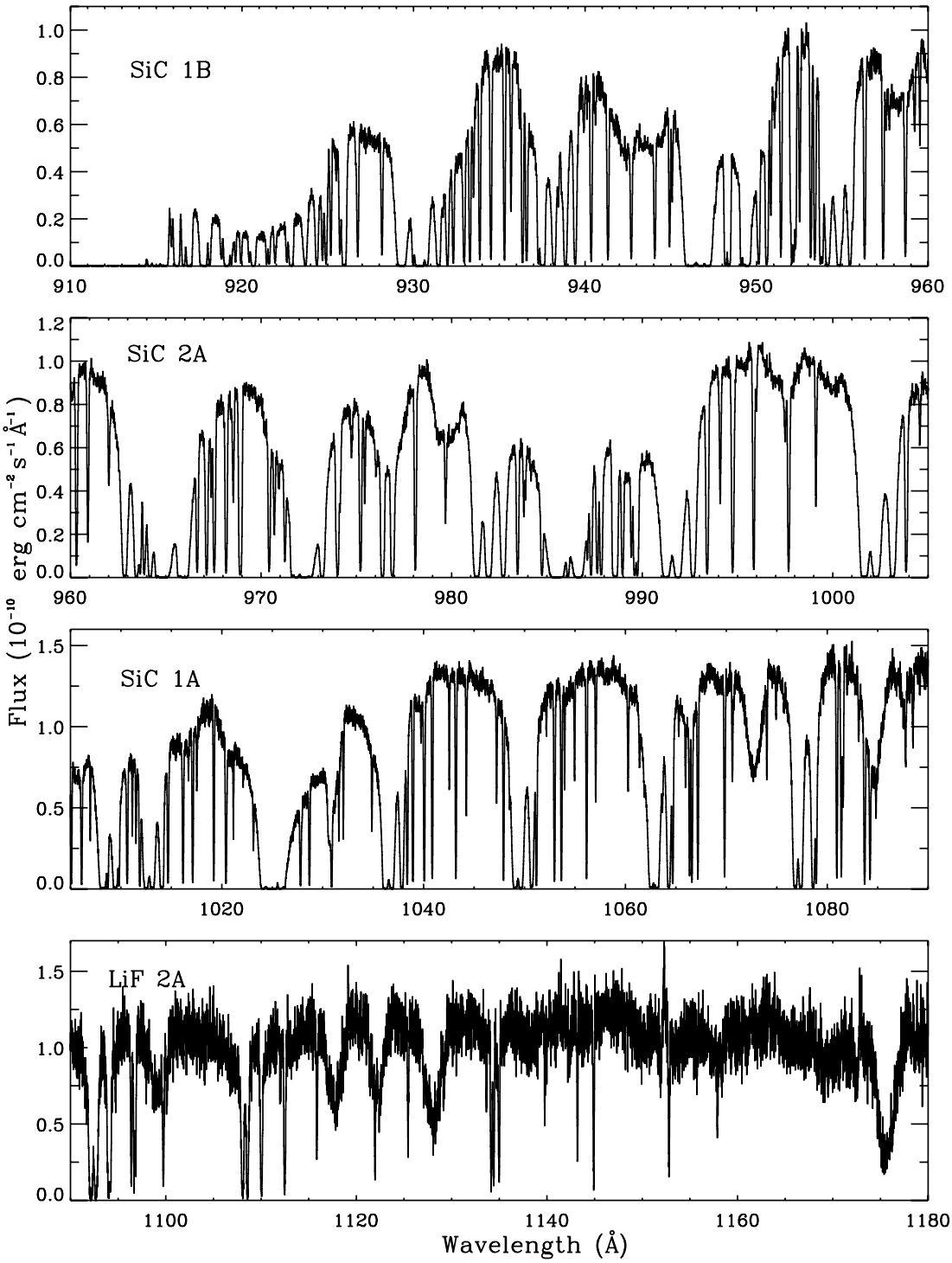

FIG. 1.—*FUSE* spectrum of HD 41161. The *FUSE* channel used for each panel is indicated at the top left. The SiC data displayed is from the MDRS observation; the LiF one is from the LWRS observation (no LiF data obtained in the MDRS observation; see Table 2).

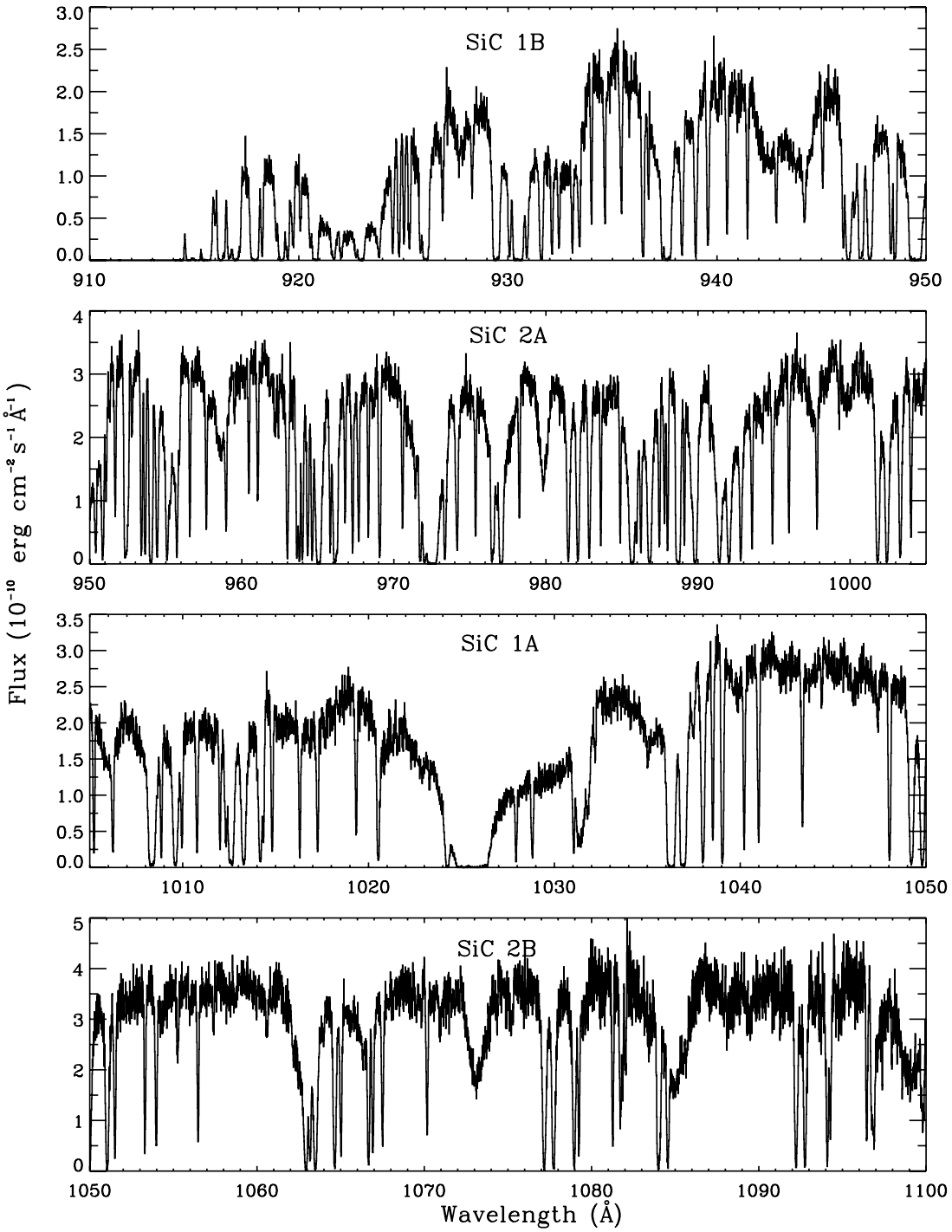

FIG. 2.—*FUSE* spectrum of HD 53975. The *FUSE* channel used for each panel is indicated at the top, in the center. No LiF data was obtained for this target.

TABLE 3
ATOMIC DATA AND EQUIVALENT WIDTHS (m Å) FOR THE LINES USED IN THE ANALYSES

Species	Wavelength (Å)	log $f\lambda$	HD 41161	HD 53975
D I	916.1785	−0.28	(A, P)	(A, P)
	916.9311	−0.18	...	(P)
	917.8797	−0.07	(P)	...
	919.1013	0.04	...	(P)
	920.713	0.17	...	(A, P)
C I	945.1910	2.16	89.59 ± 2.55 (A)	51.37 ± 4.30 (A)
C III	977.0200	2.87	222.90 ± 6.22 (A)	311.13 ± 17.61 (A)
N I	951.0792	−0.79	67.53 ± 2.42 (C, P)	49.96 ± 4.01 (C, P)
	951.2948	−1.66	18.52 ± 1.95 (A, C, P)	24.68 ± 3.76 (C, P)
	953.4152	1.09	126.05 ± 2.37 (C)	144.00 ± 3.45 (C)
	953.6549	1.37	132.32 ± 2.60 (C)	147.30 ± 3.41 (C)
	959.4937	−1.30	28.89 ± 1.26 (C, P)	22.55 ± 2.39 (A, C, P)
	960.2014	−1.95	...	(P)
	963.9903	1.08	...	154.30 ± 5.03 (C)
	964.6256	0.88	...	128.36 ± 8.29 (C)
	1134.1653	1.22	158.26 ± 4.92 (C)	...
	1134.4149	1.51	162.92 ± 5.15 (C)	...
	1134.9803	1.67	180.55 ± 6.35 (C)	...
N II	1083.994	2.10	170.00 ± 4.94 (A)	244.55 ± 9.95 (A)
O I	974.070	−1.82	(P)	(P)
O VI	1031.9261	2.13	...	91.16 ± 12.84 (P)
	1037.6167	1.83	...	42.92 ± 7.22 (A, P)
Mg II	946.7033	−0.17	...	(P)
	946.7694	−0.48	...	(P)
P II	961.0412	2.53	74.90 ± 2.23 (A)	88.23 ± 4.74 (A)
S III	1012.4950	1.65	...	86.38 ± 10.13 (P)
Cl I	1088.0589	1.95	44.55 ± 1.97 (A)	14.16 ± 3.46 (A)
Cl II	1071.0358	1.21	16.16 ± 0.96 (A)	...
Ar I	1066.6599	1.86	114.17 ± 3.03 (A)	158.12 ± 7.86 (A)
Ar II	919.7810	0.91	...	(P)
Fe II	926.8969	0.72	...	19.76 ± 2.06 (C, P)
	1055.2617	0.90	46.34 ± 1.31 (C, P)	46.33 ± 2.44 (A, C, P)
	1062.1517	0.49	17.59 ± 2.17 (C, P)	...
	1063.9718	0.60	20.41 ± 2.19 (C)	19.18 ± 3.70 (A, C)
	1081.8748	1.13	88.26 ± 2.36 (C)	61.79 ± 3.59 (C)
	1083.4204	0.48	27.75 ± 2.22 (C, P)	...
	1096.8770	1.55	93.16 ± 3.03 (C)	...
	1112.0480	0.84	34.34 ± 3.78 (C)	...
	1121.9749	1.36	83.15 ± 5.79 (C)	...
	1125.448	1.26	84.07 ± 4.35 (C)	...
	1127.0984	0.50	25.86 ± 5.16 (A, C)	...
	1133.6654	0.80	50.57 ± 3.73 (A, C, P)	...
	1142.3656	0.68	45.39 ± 4.79 (C, P)	...
	1143.2260	1.31	80.79 ± 4.64 (C, P)	...
	1144.938	2.08	122.30 ± 5.36 (C)	...

NOTE.—A, C, and P indicate which methods were used with each transition and stand for apparent optical depth, curve of growth, and profile fitting, respectively.

given the S/N of the *Copernicus* data near the O VI λ1032 transition, it is likely that the two determinations are compatible.

Cl I is also detected along the HD 41161 sight line. We use the λ1088 Cl I transition to determine N(Cl I) along this sight line with the AOD method. Besides the λ1088 transition, many other Cl I transitions (for which only theoretically derived oscillator strengths are available) are detected. The high S/N of the data allows us to place constraints on the f-values of several of these transitions. This is discussed in detail in § 7.

4.2. H_2 *and* HD *along the Line of Sight to HD 41161*

Absorption by molecular hydrogen from the rotational levels $J = 0$ through $J = 5$ and by HD ($J = 0$) is present in the spectra of HD 41161. We use the AOD technique to determine the column densities of HD ($J = 0$) and H_2 ($J = 4$ and $J = 5$).

We fit a single-b COG to the measured equivalent widths of HD and H_2 ($J = 1$–5) for the HD 41161 sight line. Transitions from the rotational level $J = 0$ are too blended with those of other species to allow measurements of equivalent widths. We determine $b_{H_2} = 7.2^{+0.4}_{-0.2}$ km s^{-1}.

We use the PF technique to determine the column densities of HD and H_2 along this sight line by fitting one absorption component simultaneously to multiple transitions of HD and H_2. We derive $b_{H_2} \sim 7$ km s^{-1}.

Table 5 presents the adopted molecular column densities along this sight line (following the same reasoning above, used to adopt

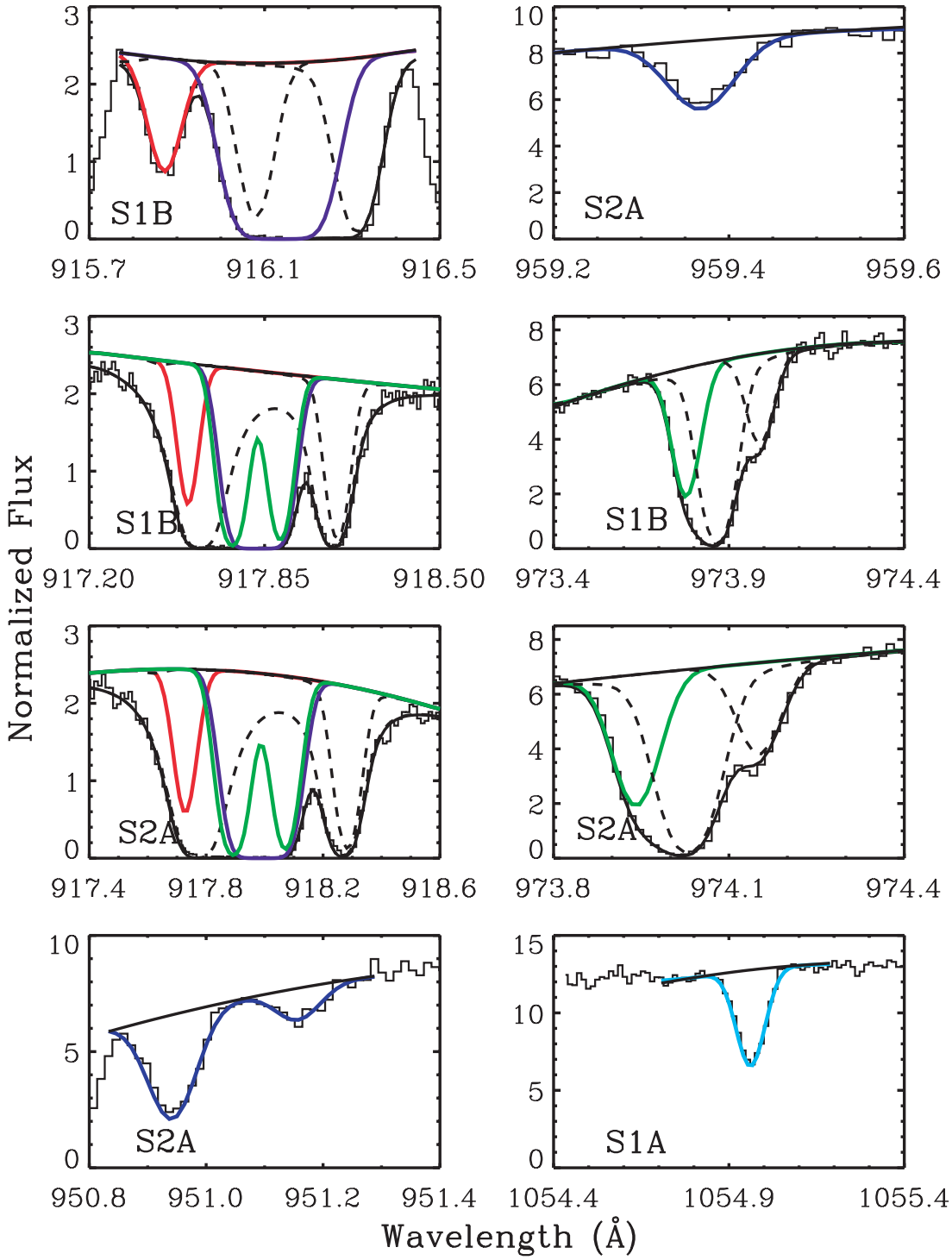

FIG. 3.—Fits to some of the lines used to determine column densities along the HD 41161 sight line (convolved with the instrument LSF). Absorption by H I is represented by magenta, D I by red, N I by dark blue, O I by green, and Fe II by cyan. Absorption by H_2 is represented by black dashed lines. See § 4.1 for discussion.

TABLE 4
Atomic Column Densities (log) for HD 41161

Species	AOD	COG	PF	Adopted
H I	...	...	...	21.00 ± 0.09[a]
D I	16.37 ± 0.04 (λ916.18)	...	16.43 ± 0.03	16.40 ± 0.05
N I	17.06 ± 0.04 (λ951.29)	$17.00^{+0.04}_{-0.03}$	16.94 ± 0.01	17.00 ± 0.06
O I	...	...	18.04 ± 0.05	18.04 ± 0.05
Fe II	$14.96^{+0.08}_{-0.10}$ (λ1127)	15.02 ± 0.06	14.94 ± 0.03	14.98 ± 0.06
Cl I	13.72 ± 0.04 (λ1088)	...	...	13.72 ± 0.04
C I	$\geq$14.13 (λ945)	...	...	$\geq$14.13
C III	$\geq$14.04 (λ977)	...	...	$\geq$14.04
N II	$\geq$14.52 (λ1083)	...	...	$\geq$14.52
P II	$\geq$13.63 (λ961)	...	...	$\geq$13.63
Cl II	$\geq$14.02 (λ1071)	...	...	$\geq$14.02
Ar I	$\geq$14.52 (λ1066)	...	...	$\geq$14.52

Note.—All uncertainties are 1 σ.
[a] See § 2.1.

the atomic column densities for this sight line). Our results agree with those derived by Dixon et al. (1998), except for $J = 2$, for which they quote $\log N(J = 2) = 17.6 \pm 0.2$, while we find $\log N(J = 2) = 17.97 \pm 0.10$. We find $\log N(\mathrm{H_2}) = 19.98 \pm 0.08$. Using the column densities for the $J = 0$ and $J = 1$ levels, we derive the excitation temperature $T_{01} = 84 \pm 7$ K. This temperature is in good agreement with that found by Savage et al. (1977) from *Copernicus* observations of 61 sight lines with $\log N(\mathrm{H_2}) > 18.0$ (77 ± 17 K) and that derived by Rachford et al. (2002) from a *FUSE* survey of sight lines with $A_v \geq 1$ mag (68 ± 15 K).

We derive $\log N(\mathrm{H_2}) = 19.98^{+0.08}_{-0.09}$, which, combined with N(H I) from § 2.1, leads to the total hydrogen column density along this sight line $\log N(\mathrm{H}) = \log[N(\mathrm{H\ I}) + 2N(\mathrm{H_2})] = 21.08 \pm 0.08$, and to the molecular fraction $f_{\mathrm{H_2}} = 2N(\mathrm{H_2})/N(\mathrm{H}) = (16.0^{+4.0}_{-3.4})\%$.

4.3. *Atomic Species along the Line of Sight to HD 53975*

The AOD technique is used to place lower limits on the column densities of C I, C III, N II, P II, S III, and Ar I, and to determine column densities of D I, N I, O VI, Fe II, and Cl I along the HD 53975 sight line.

We use the COG method to derive column densities of N I and Fe II along the HD 53975 sight line. We derive $b_{\mathrm{N\ I}} = 9.6 \pm 0.4$ km s^{-1} and $b_{\mathrm{Fe\ II}} \sim 12$ km s^{-1}.

With the PF technique we fit a single absorption component to the low-ionization atomic species D I, N I, O I, Fe II, and Mg II, and another to the molecular species. H I is included in the fit as well, in a separate absorption component, with the sole purpose of modeling the continuum in the vicinity of the D I lines. A separate component is used to model the absorption by O VI. We use an LSF with a FWHM of 0.0641 Å to fit the *FUSE* data, constant for all channels and wavelengths, corresponding to a spectral resolution of $\sim$20 km s^{-1}. Figure 4 presents fits to some of the lines used to determine the column densities along this sight line. We derive $b \sim 15$ km s^{-1} for the absorption component containing D I. Similarly to HD 41161, this Doppler parameter reflects the broadening of the lines due to multiple unresolved absorption components along the line of sight. From the four D I transitions used to constrain N(D I) (see Table 3), only the λ916.9 line suffers from major blends with $\mathrm{H_2}$ ($J = 3$), whose column density is not well constrained (see § 4.4 below). Removing this D I line from the fits does not affect the N(D I) value adopted. Table 6 presents the atomic column densities along this sight line obtained with the different methods, as well as the adopted values (see § 4.1 for how values and uncertainties are adopted).

TABLE 5
Molecular Column Densities (log)

Species	Level	HD 41161	HD 53975
HD	$J = 0$	14.57 ± 0.08	13.42 ± 0.10
$\mathrm{H_2}$	$J = 0$	19.63 ± 0.06	18.79 ± 0.05
	$J = 1$	19.72 ± 0.06	18.95 ± 0.05
	$J = 2$	17.97 ± 0.10	17.8:
	$J = 3$	17.40 ± 0.10	17.7:
	$J = 4$	14.95 ± 0.08	14.33 ± 0.05
	$J = 5$	14.34 ± 0.05	13.80 ± 0.05
$N(\mathrm{H_2})$	...	$19.98^{+0.08}_{-0.09}$	19.18 ± 0.04
N(H)	...	21.08 ± 0.08	21.14 ± 0.06

Note.—All uncertainties are 1 σ.

4.4. $\mathrm{H_2}$ *and* HD *along the Line of Sight to HD 53975*

Absorption by HD and by molecular hydrogen from the rotational levels $J = 0$ through $J = 5$ is detected along this sight line. We use the AOD technique to determine the column densities of the $\mathrm{H_2}$ $J = 4$ and $J = 5$ levels.

Similarly to HD 41161, we fit a single-b COG to the measured equivalent widths of $\mathrm{H_2}$ ($J = 0$–5), and we use the PF method to determine the column densities of the different $\mathrm{H_2}$ J levels and HD by fitting one absorption component to $\mathrm{H_2}$ and HD. We find that the column densities of the levels $J = 0$ through $J = 3$ derived with the COG method are at least a factor of $\sim$2 larger than the ones derived with the PF technique. An $\mathrm{H_2}$ absorption model containing the column densities and Doppler parameter derived with the single-b COG leads to $\mathrm{H_2}$ absorption profiles that are inconsistent with the data and that clearly overestimate the true $N(\mathrm{H_2})$ along this sight line. For this reason we adopt for $N(\mathrm{H_2})$ along this sight line the results derived with the AOD and PF techniques. Transitions from the $J = 2$ and $J = 3$ rotational levels are on the flat part of the COG; hence, the associated column densities are very uncertain and are flagged with ":" in Table 5.

We note that N(D I) is not affected by the adopted $N(\mathrm{H_2})$, as fits performed where the D I lines blended with $\mathrm{H_2}$ were removed from the fit (particularly λ916.9) lead to a N(D I) consistent with the value adopted in Table 6.

Table 5 presents the adopted molecular column densities for this sight line (see § 4.1 for how values and uncertainties are

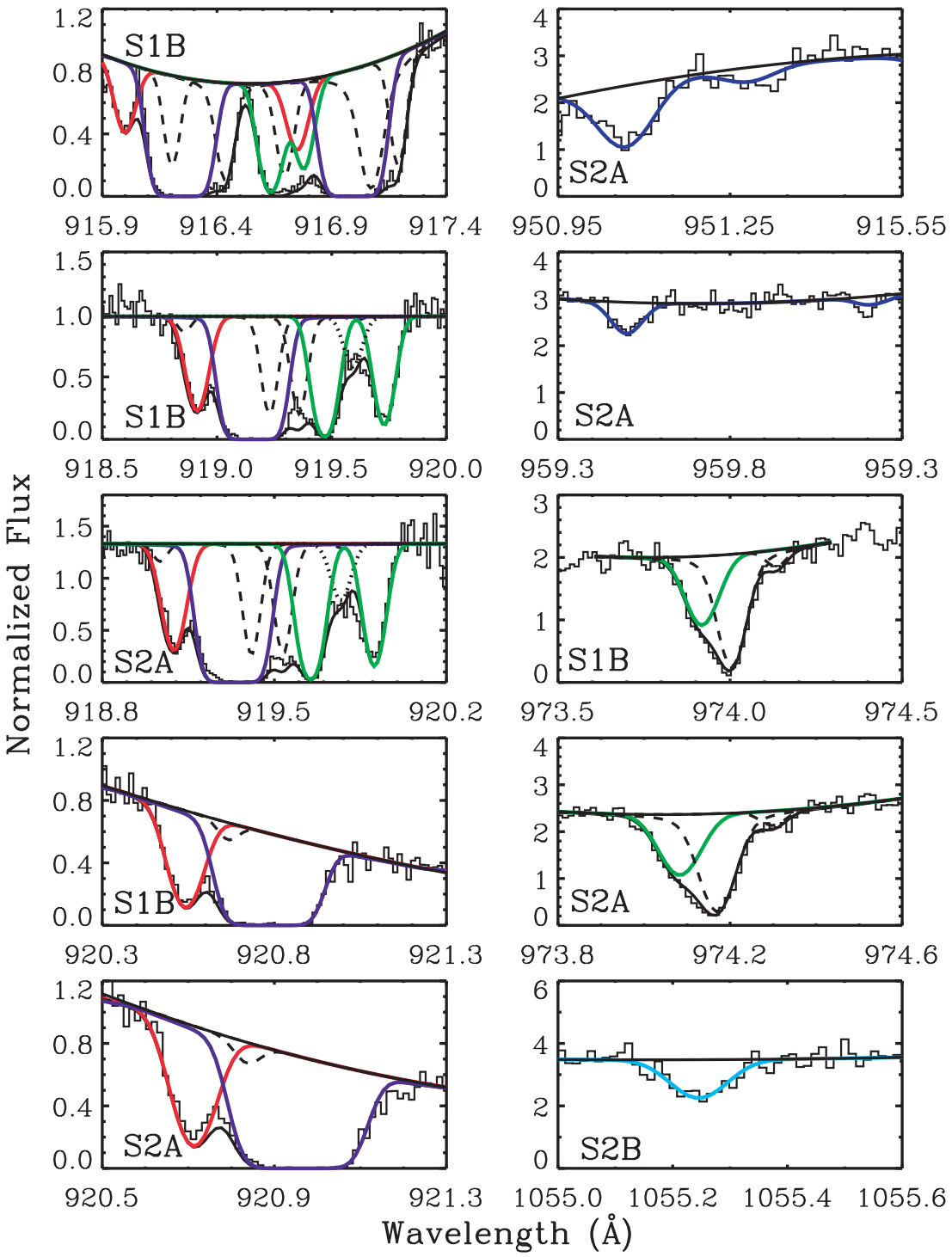

FIG. 4.—Fit of some of the lines used to determine column densities along the HD 53975 sight line (convolved with the instrument LSF). Colors are the same as in Fig. 3. Absorption by Ar II is represented by a black dotted line. See § 4.3 for discussion.

adopted). We find $\log N(H_2) = 19.18 \pm 0.04$ by adding the column densities of the $J = 0$ and $J = 1$ levels, which contain most of the H_2 along this sight line. Using the column densities for these two levels we derive the excitation temperature $T_{01} = 93 \pm 9$ K, which is in agreement with that found by Savage et al. (1977), but slightly higher than that found by Rachford et al. (2002). The total hydrogen column density along this sight line is then $N(H) = 21.14 \pm 0.06$ with $f_{H_2} = (2.2^{+0.4}_{-0.3})\%$.

5. NEUTRAL HYDROGEN ABUNDANCES

5.1. N(H I) *along the HD 41161 Line of Sight*

To check the consistency of N(H I) determined from the Lyα transition in the *IUE* data, we use some of the H I Lyman transitions in the *FUSE* bandpass to determine N(H I) with the profile-fitting technique. The following transitions are used to constrain N(H I): $\lambda\lambda$1025, 972, 920, 918, 917, and 916. No stellar model is

TABLE 6
Atomic Column Densities (log) for HD 53975

Species	AOD	COG	PF	Adopted
H I	...	...	...	21.13 ± 0.06[a]
D I	16.11 ± 0.03 (λ920.7)	...	16.20 ± 0.02	16.15 ± 0.07
N I	16.73 ± 0.05 (λ959.49)	$16.89^{+0.10}_{-0.07}$	16.84 ± 0.05	16.80 ± 0.08
O I	...	...	17.87 ± 0.08	17.87 ± 0.08
O VI	13.97 ± 0.07 (λ1031)	...	13.96 ± 0.03	13.96 ± 0.05
Fe II	$14.80^{+0.07}_{-0.08}$ (λ1063.9)	$14.87^{+0.08}_{-0.11}$	$14.84^{+0.02}_{-0.03}$	14.84 ± 0.05
Mg II	...	...	16.10 ± 0.05	16.10 ± 0.05
Cl I	13.53 ± 0.10 (λ1088)	...	...	13.53 ± 0.10
C I	$\geq$13.73 (λ945)	...	...	$\geq$13.73
C III	$\geq$14.22 (λ977)	...	...	$\geq$14.22
N II	$\geq$14.73 (λ1083)	...	...	$\geq$14.73
P II	$\geq$13.62 (λ961)	...	...	$\geq$13.62
S III	$\geq$14.54 (λ1012)	...	...	$\geq$14.54
Ar I	$\geq$14.67 (λ1066)	...	...	$\geq$14.67

Note.—All uncertainties are 1 σ.
[a] See § 2.2.

used in conjunction with the *FUSE* data. We fit an absorption model with one component of H_2, one component containing D I, O I, Fe II, and Ar I, and another component with H I. The damped wings of the Lyβ transition constrain N(H I), while the weaker Lyman lines constrain $b_{\rm H\,I}$. In addition to fitting the Lyman lines, we include also other regions of the spectra containing absorption lines of H_2 and other atomic species to constrain the shapes of absorption lines of these species that are unresolved from the H I Lyman transitions. Figure 5 presents the fit to the Lyβ and Lyγ H I transitions along the HD 41161 sight line. The fit yields $\log N(\rm H\,I) = 21.13^{+0.04}_{-0.05}$ and $b_{\rm H\,I} \sim 14$ km s^{-1}, in reasonable agreement with the $\log N(\rm H\,I) = 21.00 \pm 0.09$ adopted (see § 2.1). Varying the degree of the polynomials used to define the continua for the Lyβ and Lyγ transitions leads to a $\log N$(H I) value that is in agreement with $21.13^{+0.04}_{-0.05}$.

5.2. N(H I) *along the HD 53975 Line of Sight*

Similarly to HD 41161, we check the consistency of the N(H I) value derived from the *IUE* and *Copernicus* data by fitting some of the Ly H I transitions in the *FUSE* bandpass. We fit an absorption model with one component of H_2, a second component with D I, N I, O I, and Fe II, and a third component containing H I. The following H I Lyman lines are used to constrain N(H I): $\lambda\lambda$916.4, 917.2, 919.3, 920.9, 972, and 1025. Figure 6 presents the resulting fits to the H I Lyβ and Lyγ transitions. We derive $\log N(\rm H\,I) = 21.19 \pm 0.01$ (formal statistical errors) and $b_{\rm H\,I} \sim 15$ km s^{-1}, in agreement with the adopted value $\log N(\rm H\,I) = 21.13 \pm 0.06$.

6. RESULTS AND DISCUSSION

Table 7 summarizes several ratios along the two sight lines. Below we discuss each ratio in detail.

6.1. D/H *Ratios*

In the discussion below, the D/H ratios are determined using $\rm D/H = [N(D) + N(HD)]/[N(H\,I) + 2N(H_2) + N(HD)]$.

6.1.1. D/H *along the HD 41161 Sight Line*

Figure 7 presents the D/H ratio as a function of $\log N$(H). Open squares represent values from the literature and the three new values from Oliveira et al. (2006; references for all the ratios can be found in this paper), and filled circles represent the ratios derived in this work. The Local Bubble D/H ratio and uncertainties are represented by horizontal solid and dashed lines. The vertical dashed line at $\log N(\rm H) = 19.2$ represents the edge of the Local Bubble, while the vertical dashed line at $\log N(\rm H) = 20.7$ represents the approximate position of a new low and constant D/H regime that was proposed by Wood et al. (2004) and Linsky et al. (2006).

There are five sight lines with $\log N(\rm H) > 20.7$ that have D/H ratios available in the literature (HD 198965, HD 191877, JL 9, LS 1274, and HD 90087; Hoopes et al. 2003; Wood et al. 2004; Hébrard et al. 2005). For these sight lines with $20.7 < \log N(\rm H) < 21.20$, the weighted mean is $\rm D/H = (0.86 \pm 0.08) \times 10^{-5}$. HD 41161 has N(H) similar to these sight lines, but a D/H ratio inconsistent by $\sim$3 σ. To make D/H along the HD 41161 sight line consistent with the weighted ratio of the other five sight lines, one would have to increase N(H) by a factor of $\sim$2.49, or $\log N$(H I) from 21.00 to $\sim$21.44. To test whether D/H along this sight line could be high due to N(H I) being underestimated, we performed fits in which $\log N$(H I) was forced to 21.44. Figure 8 presents the fits to H I Lyβ and Lyγ with $\log N$(H I) forced to 21.44. The degree of the polynomial used to fit the continuum of these two transitions is the same as the one used for the fit in which we determined $N(\rm H\,I) = 21.13^{+0.04}_{-0.05}$. However, in this case the continuum is forced to be artificially high to accommodate the higher N(H I). In addition, the fit grossly overestimates the absorption on the blue side of the core of the Lyman lines, as shown in the two bottom panels of Figure 8. To further check that $\log N(\rm H\,I) = 21.44$ overestimates the true H I absorption, we retrieved the *IUE* Lyα spectrum for the HD 41161 sight line from the MAST archive (no further processing was applied). Figure 9 presents the fit to H I Lyα forcing $\log N(\rm H\,I) = 21.44$. Similarly to the fits to Lyβ and Lyγ discussed above, forcing such a high value of N(H I) on the data forces the continuum to be artificially high and overestimates the absorption near the core of the Lyα line.

The N(H I) value adopted for this sight line is based on measurements performed by two different sets of authors (Shull & van Steenberg 1982; Diplas & Savage 1994b) who obtain similar results, although both used the same *IUE* data set. In addition, fits of the Lyβ and Lyγ H I transitions produce a N(H I) value in agreement with the value adopted in § 2.1, while forcing N(H I) to the value required to bring D/H to agree with the other low D/H measurements in the literature (discussed above) produces

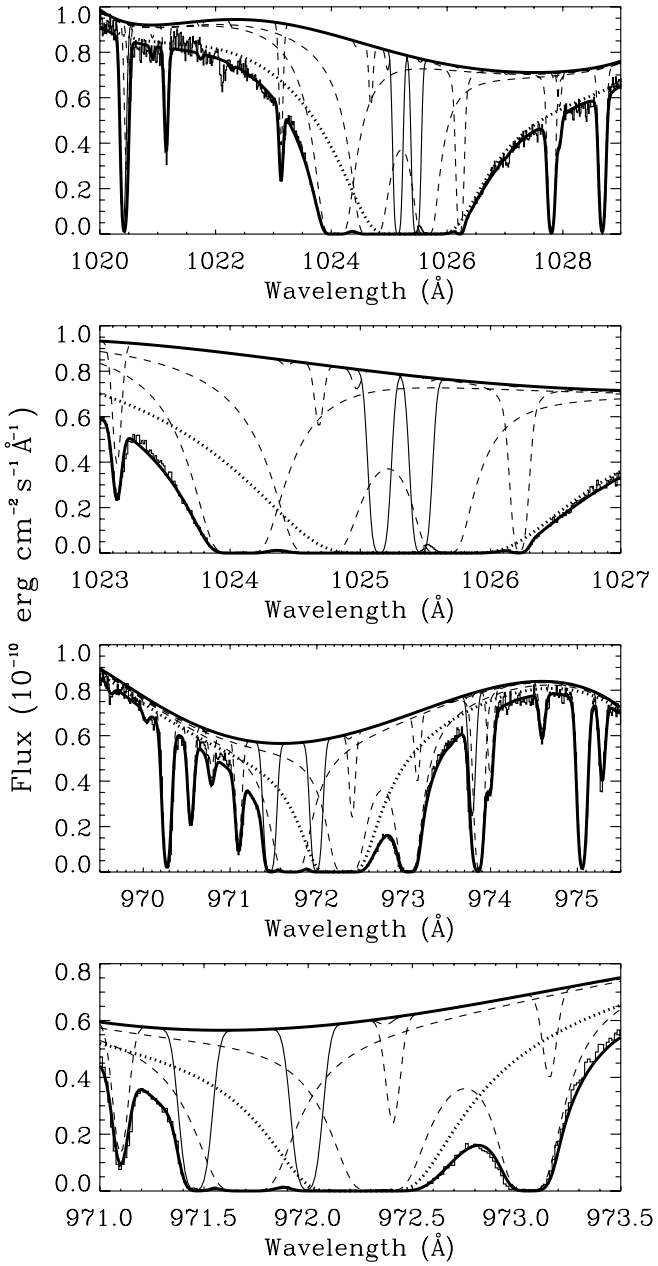

FIG. 5.—Fit to H I Lyβ (*first and second panels*) and Lyγ (*third and fourth panels*) transitions along the HD 41161 sight line, yielding $\log N(\mathrm{H\ I}) = 21.13^{+0.04}_{-0.05}$, in agreement with the value adopted in § 2.1. The cores of the Lyβ and Lyγ lines are presented in more detail in the second and fourth panels, respectively. H_2 is represented by dashed lines, O I, Si II, D I, and Fe II by thin solid lines. H I is represented by a thick dotted line. The two top panels are from S1A MDRS, while the bottom two are from S2B MDRS. The small bump near 1025.5 Å is due to airglow emission, and does not affect our measurements. See § 5.1 for discussion.

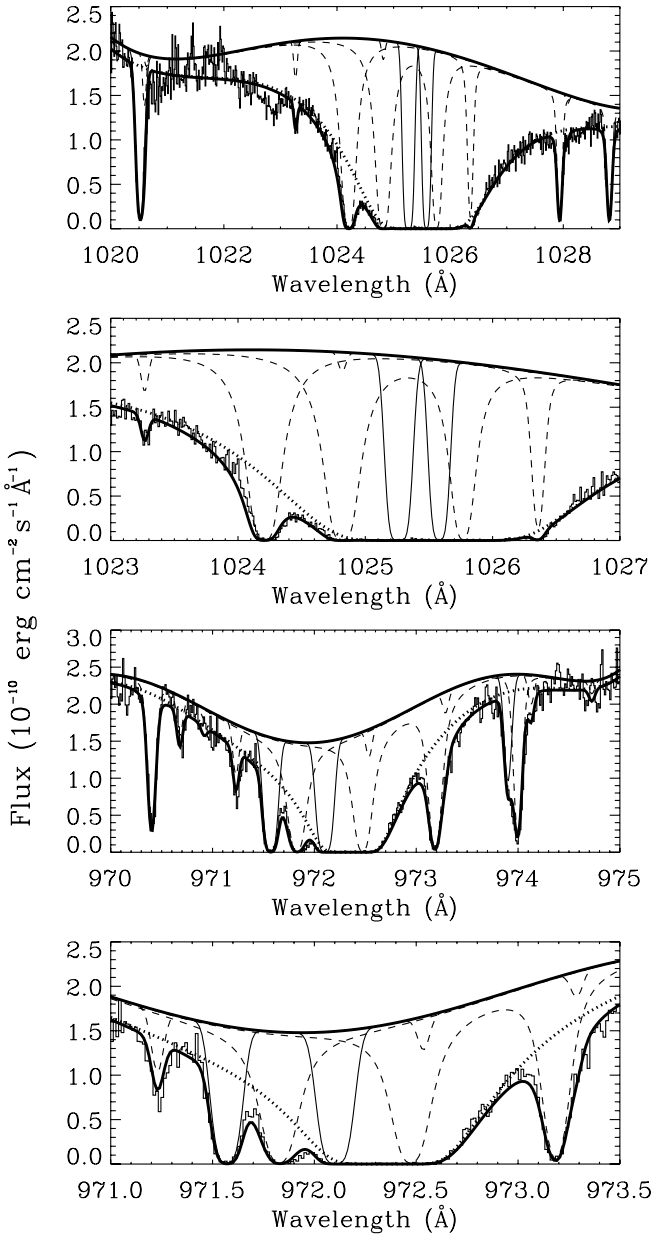

FIG. 6.—Same as Fig. 5, but for the HD 53975 sight line, yielding $\log N(\mathrm{H\ I}) = 21.19 \pm 0.01$, in agreement with the value adopted in § 2.2. The two top panels are from S1B, while the bottom two are from S1A. See § 5.2 for discussion.

fits that clearly overestimate the H I absorption. We conclude then that the high D/H along this sight line is unlikely to be due to N(H I) being underestimated.

Another possibility to explain the high D/H along this sight line is that N(D I) is overestimated. This is probably unlikely, since saturation tends to move column densities in the opposite direction, i.e., underestimation rather than overestimation. However, other factors, such as continuum placement, could produce the desired effect. A D I column density of $\log N(\mathrm{D\ I}) = 16.00$ is required to bring D/H along this sight line down to the weighted mean derived by the five sight lines discussed above. To test

TABLE 7

RATIOS OF COLUMN DENSITIES

Ratio	HD 41161	HD 53975
$(\mathrm{D/H}) \times 10^5$	$2.14^{+0.51}_{-0.43}$	$1.02^{+0.23}_{-0.20}$
$(\mathrm{N/H}) \times 10^5$	$8.32^{+2.09}_{-1.76}$	$5.07^{+1.45}_{-1.21}$
$(\mathrm{O/H}) \times 10^4$	$9.12^{+2.15}_{-1.83}$	$5.37^{+1.35}_{-1.14}$
$(\mathrm{Fe/H}) \times 10^6$	$0.79^{+0.20}_{-0.17}$	$0.50^{+0.10}_{-0.08}$
$(\mathrm{D/O}) \times 10^2$	$2.29^{+0.40}_{-0.35}$	$1.91^{+0.51}_{-0.43}$
O/N	$10.96^{+2.10}_{-1.85}$	$11.74^{+3.36}_{-2.80}$
$(\mathrm{HD/H_2}) \times 10^6$	$3.89^{+1.11}_{-0.93}$	$1.74^{+0.48}_{-0.39}$
$f_{\mathrm{H_2}}$ (%)	$16.0^{+4.0}_{-3.4}$	$2.2^{+0.4}_{-0.3}$
$\langle n_{\mathrm{H}} \rangle$ (cm^{-3})	0.31	0.34

NOTES.—All uncertainties are 1 σ and $\mathrm{D/H} = [N(\mathrm{D\ I}) + N(\mathrm{HD})]/[N(\mathrm{H\ I}) + 2N(\mathrm{H_2}) + N(\mathrm{HD})]$.

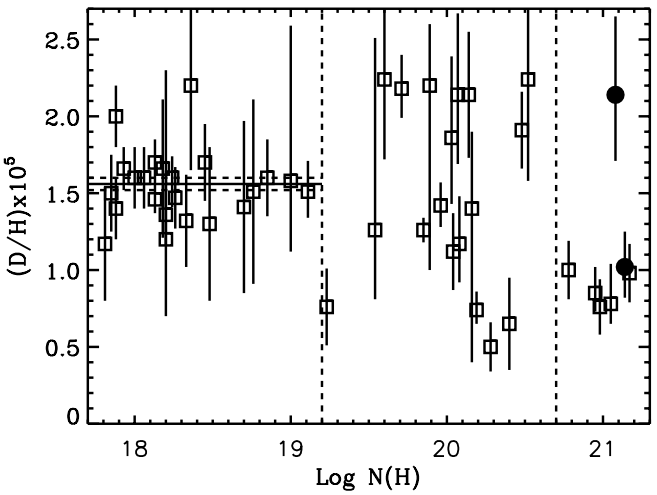

FIG. 7.—D/H as a function of $\log N(\mathrm{H})$. Open squares represent ratios from the literature and from Oliveira et al. (2006; where references to all the individual ratios presented can be found); filled circles represent the two new ratios derived in this work. Dashed and solid horizontal lines mark the Local Bubble D/H ratio $(1.56 \pm 0.04) \times 10^{-5}$ derived from a compilation of measurements by Wood et al. (2004). Dashed vertical lines mark $\log N(\mathrm{H}) = 19.2$, corresponding to the edge of the Local Bubble, and $\log N(\mathrm{H}) = 20.7$, after which Wood et al. (2004) and Linsky et al. (2006) proposed that D/H was low and constant.

whether this $N(\mathrm{D\ I})$ value is consistent with the data, we consider the $\lambda\lambda$916.18 and 919.1 D I transitions. With the AOD method, we derive $\log N(\mathrm{D\ I}) = 16.37 \pm 0.04$ from the λ916.2 transition and our fits yield $\log N(\mathrm{D\ I}) = 16.43 \pm 0.03$. A column density of $\log N(\mathrm{D\ I}) = 16.00$ clearly underestimates the true D I absorption, as shown in Figure 10, where we overplot the above column density on the λ916.2 transition.

To further check our $N(\mathrm{D\ I})$ measurement along this sight line, we can consider the λ919.1 D I transition. This transition, not used in our analysis of this sight line, is blended with H_2 ($J = 4$) and, according to our model, slightly saturated. Using our H_2 fit model, we carefully deblend the D I and H_2 transitions. We then use the AOD technique to derive a lower limit to $N(\mathrm{D\ I})$, using the deblended D I λ919.1 transition. This exercise yields $\log N(\mathrm{D\ I}) > 16.13$, indicating that it is unlikely that $N(\mathrm{D\ I})$ is overestimated.

We conclude then that the high D/H ratio along this sight line is unlikely to be due to either underestimation or overestimation of the H I or D I column densities, respectively.

According to the variable deuterium depletion model proposed by Linsky et al. (2006), sight lines that probe gas with high column densities should be biased by cold, not recently shocked gas, where deuterium would be depleted in grains. The high D/H toward HD 41161 might indicate that this scenario occurs at $N(\mathrm{H})$ higher than what was previously thought, or that the clumping of low D/H values in the literature has another explanation. There is also the possibility that this sight line is dominated by gas that has been shocked and where the typical traces of a shock, such as highly ionized species (not detected along this sight line), have been erased. In this scenario, the timescale to erase the traces of the shock would have to be smaller than that for D to deplete into the grains. The presence of cold H_2 ($T_{01} = 84 \pm 7$ K) along this sight line does not necessarily imply that the gas is cold and undisturbed, since H_2 is only a minor constituent of the sight line. Finally, we cannot rule out that local production of D I of the type proposed by Mullan & Linsky (1999) or Prodanović & Fields (2003) is responsible for all or part of the deuterium enhancement along this sight line.

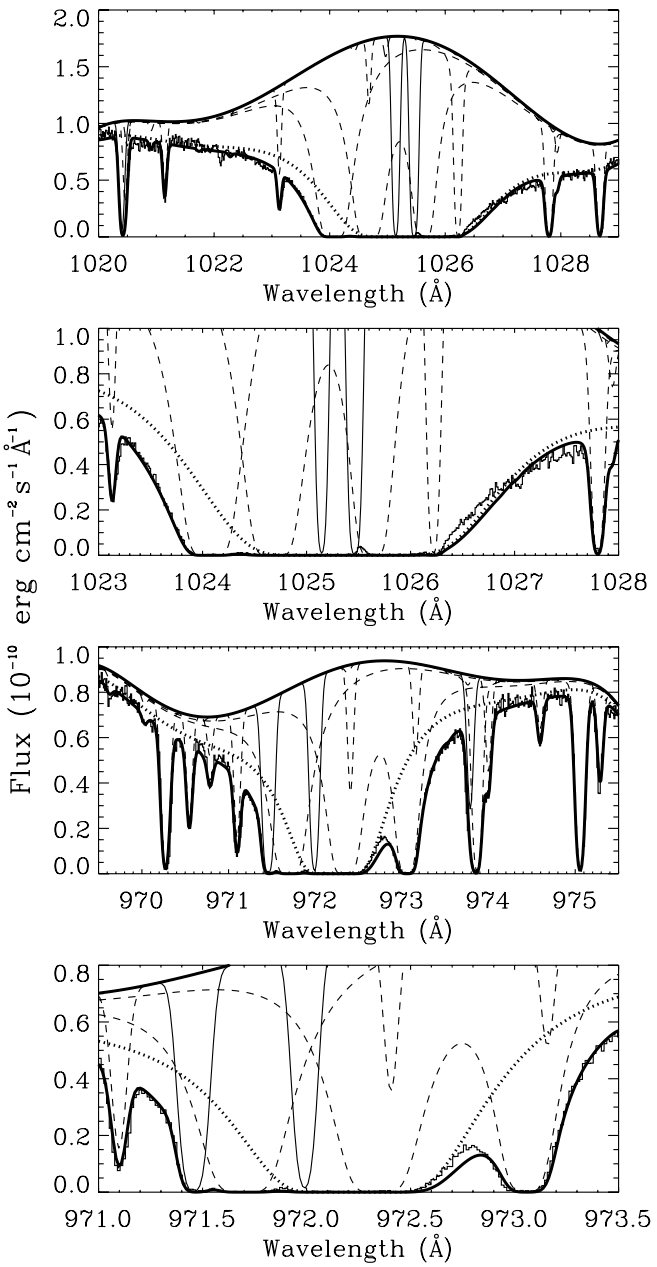

FIG. 8.—Forced fit to H I Lyβ (*first and second panels*) and Lyγ (*third and fourth panels*) transitions along the HD 41161 sight line, with $\log N(\mathrm{H\ I}) = 21.44$, required to bring D/H along this sight line to agree with D/H for five other sight lines with similar $N(\mathrm{H})$. Dashed lines represent H_2, and thin solid represent O I, Si II, D I, and Fe II. H I is represented by a thick dotted line. The two top panels are from S1A MDRS, while the bottom two are from S2B MDRS. The cores of the Lyβ and Lyγ transitions, presented in more detail in the second and fourth panels, show that $\log N(\mathrm{H\ I}) = 21.44$ clearly overestimates the true H I absorption. See § 6.1.1 for discussion.

To determine the iron depletion along this sight line, $\mathrm{D(Fe)} = \log(\mathrm{Fe/H})_{\mathrm{gas}} - \log(\mathrm{Fe/H})_{\odot}$, we use the solar abundance ratio $\log(\mathrm{Fe/H})_{\odot} = -4.55 \pm 0.05$ from Asplund et al. (2005). We find for this sight line $\mathrm{D(Fe)} = -1.55 \pm 0.11$. In a manner similar to some other sight lines with high D/H ratios, the Fe/H ratio along this sight line does not fit the trend of high Fe/H versus high D/H displayed for most of the cases shown in Figure 3 of Linsky et al. (2006). There are, however, a few sight lines in Figure 3 of the paper mentioned above that seem to follow a trend different than most of the points, in that for the same Fe depletion a higher D/H ratio is found. The D/H and Fe/H ratios

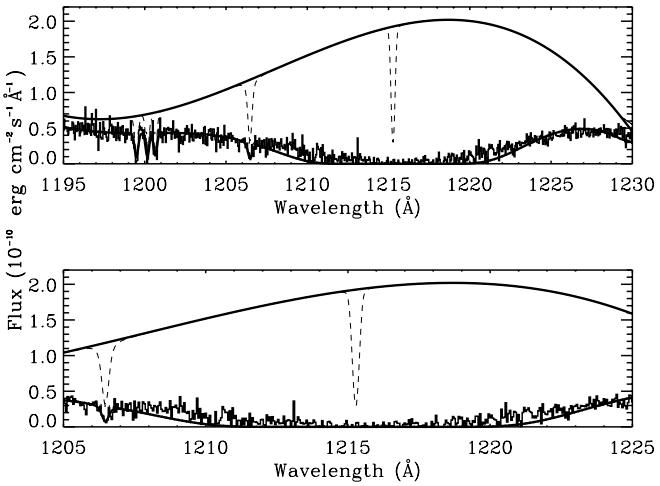

FIG. 9.—Forced fit to the H I Lyα transition along the HD 41161 sight line, with $\log N(\mathrm{H\ I}) = 21.44$, required to bring D/H along this sight line to agree with D/H for five other sight lines with similar N(H). Dashed lines represent N I, Si III, and D I. The global fit, including H I as well as the continuum, are represented by thick solid lines. The core of the Lyα transition, presented in more detail in the second panel, clearly shows that $\log N(\mathrm{H\ I}) = 21.44$ clearly overestimates the true H I absorption. See § 6.1.1 for discussion.

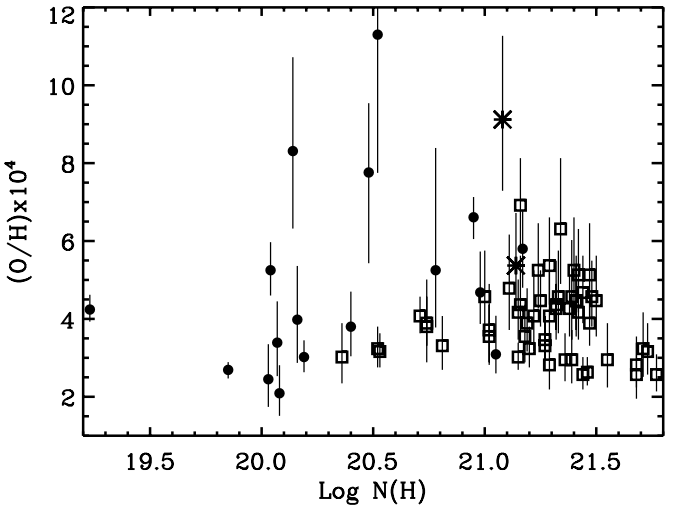

FIG. 11.—O/H as a function of $\log N$(H). Filled circles correspond to *FUSE*-based measurements from the literature (see, e.g., Oliveira et al. [2006] for a compilation of these values). The two new values derived here are represented by asterisks, and open squares represent *HST*-based measurements from Cartledge et al. (2004).

along the sight line to HD 41161 seem to follow this trend as well. Linsky et al. (2006) discuss some of the causes that could lead to this sort of behavior and argue that these sight lines could either contain a smaller percentage of carbon grains (thus fewer sites for deuterium to deplete) or could have had weak shocks pass by, which would have evaporated deuterium from the grain mantles.

6.1.2. D/H *along the HD 53975 Sight Line*

For the HD 53975 sight line we derive $\mathrm{D/H} = (1.02^{+0.23}_{-0.20}) \times 10^{-5}$, in agreement with the weighted mean $\mathrm{D/H} = (0.86 \pm 0.08) \times 10^{-5}$ quoted above. Although the D/H ratio along the HD 41161 sight line indicates that D/H is variable for $\log N(\mathrm{H}) > 20.7$, the D/H ratio along the HD 53975 sight line follows the trend displayed by the other five sight lines in the literature with $\log N(\mathrm{H}) > 20.7$. Taking into account this ratio, along with the ratios for the five sight lines mentioned above, yields a weighted mean $\mathrm{D/H} = (0.89 \pm 0.07) \times 10^{-5}$ (with $\chi^2_\nu = 0.4$ for 5 degrees of freedom; the average of the upper and lower 1 σ uncertanties of individual ratios are used to determine weighted means in this work). The iron depletion along this sight line, $D(\mathrm{Fe}) = -1.75 \pm 0.09$, follows the trend of low Fe/H versus low D/H displayed in Figure 3 of Linsky et al. (2006).

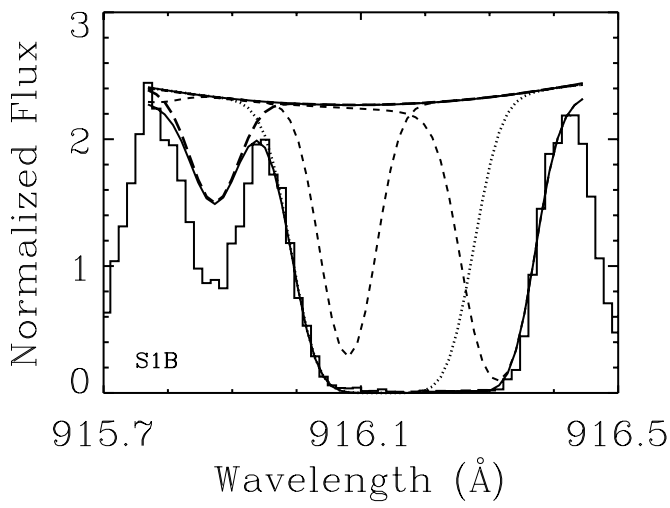

FIG. 10.—The value $\log N(\mathrm{D\ I}) = 16.00$, required to lower D/H along the HD 41161 sight line is superimposed on D I λ916.2. Absorption is represented by short-dashed lines for H I, long-dashed lines for D I, and dotted lines for H_2. The overall fit and continuum are represented by solid lines. This figure shows that $\log N(\mathrm{D\ I}) = 16.00$ clearly underestimates the true D I absorption. Compare this figure to the corresponding panel in Fig. 3, where we derive $\log N(\mathrm{D\ I}) = 16.43 \pm 0.03$. See § 6.1.1 for discussion.

6.2. O/H *Ratios*

The O/H ratio along the HD 41161 sight line, $\mathrm{O/H} = (9.12^{+2.15}_{-1.83}) \times 10^{-4}$, is more than 3 σ away from $\mathrm{O/H} = (3.43 \pm 0.15) \times 10^{-4}$ derived for 13 lines of sight probing gas within 1500 pc (most within 500 pc), with $20.18 \leq \log N(\mathrm{H\ I}) \leq 21.28$ by Meyer et al. (1998; updated f-value). For HD 53975, $\mathrm{O/H} = (5.37^{+1.35}_{-1.14}) \times 10^{-4}$, is $\sim$1.7 σ away from the Meyer et al. (1998) O/H ratio. The *FUSE*-based O/H measurements present a larger scatter than those based on *HST* data (see, for example, André et al. 2003; Cartledge et al. 2004). Figure 11 presents a compilation of O/H measurements performed with *FUSE* (from this work and the compilation by Oliveira et al. [2006]; *asterisks and filled circles*, *respectively*) and *HST* data (from Cartledge et al. [2004]; *open squares*). For the *FUSE* measurements we consider only sight lines that probe gas beyond the Local Bubble, i.e., $\log N(\mathrm{H}) > 19.2$, since previous measurements by Oliveira et al. (2005) have shown that $\mathrm{O/H} = (3.45 \pm 0.19) \times 10^{-4}$ in the LB. The assumption that all the *HST* O/H measurements can be described by a single mean leads to the weighted mean $\mathrm{O/H} = (3.51 \pm 0.10) \times 10^{-4}$, with $\chi^2_\nu = 1.35$, for 51 degrees of freedom. Assuming that the *FUSE* measurements can also be described by a single mean leads to the weighted mean $\mathrm{O/H} = (3.56 \pm 0.13) \times 10^{-4}$, but with $\chi^2_\nu = 5.4$ for 18 degrees of freedom. The scatter in the *FUSE* O/H measurements is more pronounced in the range $20.0 \leq \log N(\mathrm{H}) \leq 20.9$, where there are only a few *HST* measurements available. Hence, the scatter in the *FUSE* measurements might be due to there really being more scatter for lower column density sight lines, even if the O/H values for the LB show little scatter (Oliveira et al. 2005).

The larger (than Meyer et al. 1998) sample of sight lines probed by the work of Cartledge et al. (2004) contains some sight lines

with O/H ratios $\sim 6 \times 10^{-4}$. For example, HD 91824 ($l = 285\overset{\circ}{.}70, b = 0\overset{\circ}{.}07$) and HD 91983 ($l = 285\overset{\circ}{.}88, b = 0\overset{\circ}{.}05$) are both members of the Carina OB1 association (located at $d \sim 2.5$ kpc) and have $\mathrm{O/H} = (6.91^{+1.21}_{-0.92}) \times 10^{-4}$ and $(5.25^{+1.21}_{-0.98}) \times 10^{-4}$, respectively (Cartledge et al. [2004], based on *HST* data). HD 90087 ($l = 285\overset{\circ}{.}16, b = -2\overset{\circ}{.}13$) is also part of the Carina OB1 association, and is $\sim$100 pc away from the two other stars. For this sight line the *FUSE*-derived $\mathrm{O/H} = (5.8 \pm 1.0) \times 10^{-4}$ (Hébrard et al. 2005) is in good agreement with the O/H ratios derived for the other members of this association.

In view of the Cartledge et al. (2004) measurements, the O/H ratio along the HD 53975 sight line does not seem to be abnormally high; however, the ratio along the line of sight to HD 41161 does. N(O I) is determined using the only unsaturated O I transition in the *FUSE* bandpass, λ974, which is heavily blended with H_2 $J = 2$ and $J = 5$. One might suspect that an erroneous f-value would lead to an inaccurate N(O I). However, previous studies by Hébrard et al. (2005) indicate that N(O I) derived from this transition is consistent with N(O I) derived both from weaker and stronger O I transitions. Unknown blends with stellar lines are also the unlikely cause of a seemingly high N(O I), due to the high $v_{\sin i}$ of HD 41161. We suspect that unknown systematic effects when deriving N(O I) from the heavily blended λ974 O I transition might be responsible for at least part of the scatter in the *FUSE*-based O/H measurements.

6.3. N/H, O/N, *and* D/O *Ratios*

We derive $\mathrm{N/H} = (8.32^{+2.09}_{-1.76}) \times 10^{-5}$ and $\mathrm{N/H} = (5.07^{+1.45}_{-1.21}) \times 10^{-5}$ for the HD 41161 and HD 53975 sight lines, respectively. The first ratio is consistent within the uncertainties with $\mathrm{N/H} = (7.5 \pm 0.4) \times 10^{-5}$, derived by Meyer et al. (1997). The N/H ratio for the HD 53975 sight line is $\sim$1.7 σ away from the Meyer et al. (1997) value.

We derive $\mathrm{O/N} = 10.96^{+2.10}_{-1.85}$ and $\mathrm{O/N} = 11.74^{+3.36}_{-2.80}$ along the HD 41161 and HD 53975 sight lines, respectively. The O/N ratios for HD 41161 and HD 53975 are more than 3 and 2.7 σ, respectively, away from $\mathrm{O/N} = 4.1 \pm 0.3$, derived using the values of O/H and N/H determined by Meyer et al. (1998, 1997). This is likely a consequence of the high O/H for the two sight lines, in addition to the low N/H for the HD 53975 sight line.

We derive $\mathrm{D/O} = (2.29^{+0.40}_{-0.35}) \times 10^{-2}$ and $\mathrm{D/O} = (1.91^{+0.51}_{-0.43}) \times 10^{-2}$ along the HD 41161 and HD 53975 sight lines, respectively. Both of these ratios are consistent within the uncertainties with the weighted average $\mathrm{D/O} = (1.75 \pm 0.18) \times 10^{-2}$ derived by Hébrard et al. (2005) for the distant sight lines. The low dispersion of D/O at high N(H) has been used by Hébrard & Moos (2003) and Hébrard (2006) as an argument against a high D/H ratio being representative of the ISM in the solar neighborhood. However, as pointed out above, the large scatter in the *FUSE*-derived O/H ratios seems to indicate that N(O I) might suffer from unknown systematic errors, which would affect the derived D/O ratios. If the high value of N(O I) measured along the HD 41161 sight line is indeed too high due to systematic effects related to using the λ974 transition, then the D/O ratio along this sight line would be have to be revised upwards, becoming inconsistent with the Hébrard et al. (2005) D/O ratio for distant sight lines. This would be consistent with our claim, from D/H, that the deuterium abundance toward HD 41161 is higher than that along the other $\log N(\mathrm{H}) > 20.7$ sight lines.

Finally, we would like to point out that there are other sight lines in which high-D/H, low-D/O, and high-O/H ratios are also observed, similar to the HD 41161 sight line. These are Feige 110 (Friedman et al. 2002; Hébrard et al. 2005), PG 0038+199 (Williger et al. 2005), and LSE 44 (Friedman et al. 2006). Discussions about the possible causes of these ratios are given in the papers quoted for each sight line.

7. f-VALUES OF CHLORINE

Chlorine has a unique chemistry, in so far as it can react exothermically with molecular hydrogen. Chlorine is ionized in regions where hydrogen is mostly in the atomic form, whereas in regions where there is a significant amount of molecular hydrogen, chlorine is mostly neutral, with a small fraction in the HCl molecular form (Jura 1974; Jura & York 1978); Cl I traces the cold molecular components along the sight lines. Determining accurate Cl I column densities requires accurate oscillator strengths; however, only a few transitions have experimentally determined f-values. The *FUSE* bandpass contains numerous transitions of Cl I, many of which are detected along the HD 41161 sight line. In addition, the strong λ1347 Cl I transition is also detected in the *IUE* data for this star. Schectman et al. (1993) determined the f-values of several Cl I transitions using beam-foil spectroscopy. While the f-value of Cl I λ1347 had been previously measured experimentally, $\lambda\lambda$1088, and 1097 had only theoretically determined f-values. The work by Schectman et al. (1993) presents then the first and only (up to now) experimental measurement of the f-values of the $\lambda\lambda$1088 and 1097 transitions, and the most accurate measurement of the f-value of λ1347.

Using two Cl I transitions that have experimentally determined f-values ($\lambda\lambda$1088 and 1347), we place constraints on the f-values of other transitions whose currently adopted theoretical f-values (see Morton 2003 and references therein) are obviously incorrect. For two transitions that are optically thin, i.e., on the linear part of the COG, one can derive the relationship between their equivalent widths, $W_{\lambda_1}/W_{\lambda_2} = (f_1\lambda_1^2)/(f_2\lambda_2^2)$. We can then use the wavelengths and experimentally derived f-values (as well as their associated uncertainties) for the $\lambda\lambda$1088 and 1347 Cl I transitions to derive the predicted ratio $(W_{1347}/W_{1088})_{\mathrm{pred}}$. Table 8 presents the atomic data and equivalent widths of the Cl I transitions detected along the HD 41161 sight line, as well as 1 σ upper limits on the equivalent widths of nondetected transitions. The fourth column in the table lists the references for the f-values. Using the data on this table, we derive $(W_{1347}/W_{1088})_{\mathrm{pred}} = 2.90 \pm 0.33$ under the assumption that for the HD 41161 sight line these two transitions lie in the linear part of the COG. Using the measured equivalent widths and their uncertainties from Table 8 for these two transitions we derive $(W_{1347}/W_{1088})_{\mathrm{meas}} = 2.35 \pm 0.41$. The agreement between the predicted and measured equivalent width ratios indicates that the linear COG assumption is a valid approximation for this sight line. Since Cl I traces the cooler components of a cloud, where hydrogen is mostly in molecular form, it is possible that there are more than one Cl I component not resolved by *FUSE*. However, as shown by Jenkins (1986), there are cases in which the combined equivalent widths of a population of Gaussian-like interstellar absorption components exhibit a COG that closely mimics that of a single, pure Gaussian distribution in velocity.

Although it seems that the approach above is valid for this sight line, we take a conservative viewpoint by assuming that Cl I λ1347 could be mildly saturated, but that Cl I λ1088 is not. We use then the equivalent width of this transition, as well as its uncertainty, to predict the f-values of the other weaker Cl I transitions quoted in Table 8 using the laboratory-measured f_{1088} and its uncertainty. For the transition x, the predicted f_x is then $f_x = f_{1088}(W_x/W_{1088})(\lambda_{1088}/\lambda_x)^2$. Blending of Cl I lines with stellar lines is not a concern for this sight line due to the high $v_{\sin i}$ of this star (see Table 1). In addition, careful modeling of the H_2 and HD absorption along this sight line assures us that the Cl I lines studied here are free from blends with

TABLE 8
EQUIVALENT WIDTHS AND ATOMIC DATA FOR Cl I ALONG THE HD 41161 SIGHT LINE

Wavelength (Å)	f	Reference	W_λ (mÅ)	$f_{\rm pred}$[a]
969.9195.....	1.73×10^{-2}	1	4.38 ± 0.93	$(1.0 \pm 0.2) \times 10^{-2}$
984.2865[b].....	2.44×10^{-2}	1, 2	13.18 ± 1.95	$(2.9 \pm 0.5) \times 10^{-2}$
1004.6776.....	1.58×10^{-1}	1, 2	28.63 ± 1.39	$(6.1 \pm 0.7) \times 10^{-2}$
1022.0478.....	1.22×10^{-2}	1	9.35 ± 1.24	$(1.9 \pm 0.3) \times 10^{-2}$
1027.3386.....	6.58×10^{-3}	1	12.08 ± 2.97	$(2.5 \pm 0.7) \times 10^{-2}$
1031.5070.....	1.51×10^{-1}	1, 3	10.23 ± 3.42	$(2.1 \pm 0.7) \times 10^{-2}$
1085.3035.....	5.81×10^{-4}	3, 4	12.32 ± 2.16	$(2.2 \pm 0.5) \times 10^{-2}$
1088.0589.....	$(8.1 \pm 0.7) \times 10^{-2}$	3, 5	44.55 ± 1.97	...
1094.7686.....	1.66×10^{-2}	3, 4	40.21 ± 3.04	$(7.2 \pm 0.9) \times 10^{-2}$
1347.2396.....	$(1.53 \pm 0.11) \times 10^{-1}$	3, 5	104.9 ± 17.4	...
978.5932.....	1.85×10^{-1}	1, 3	<4.5	$<1.0 \times 10^{-2}$
1043.9860.....	1.81×10^{-2}	1, 3	<2.7	$<5.3 \times 10^{-3}$
1079.8821.....	6.98 × 10−3	3, 4	<4.1	$<7.5 \times 10^{-3}$
1099.5230.....	1.14×10^{-2}	3, 4	<10.0	$<1.8 \times 10^{-2}$
1101.9361.....	1.13×10^{-2}	3, 4	<5.1	$<9.1 \times 10^{-3}$

NOTE.—For the last six transitions we quote 1 σ upper limits on the equivalent widths.
[a] See § 7 for a discussion of how $f_{\rm pred}$ is calculated.
[b] Possibly blended with the λ984.323 transition.
REFERENCES.—(1) Kurucz & Peytremann 1975; (2) Morton 1991; (3) Morton 2003; (4) Biemont et al. 1994; (5) Schectman et al. 1993. References 1–3 refer to the original papers. References 4 and 5 are compilations of atomic data.

these molecular species. In particular, the λ1088 Cl I transition, which falls near a CO transition (λ1087.868), is not affected by a blend with this molecular species, as $\log N({\rm CO}) < 13.5$ along this sight line. The last column in Table 8 presents the predicted f-values (and 1 σ uncertainties) using the equation above, which can then be compared to the f-values from the literature quoted in the second column of this table.

Our results, presented in the last column of Table 8, indicate that some Cl I transitions need to have their f-values revised by large factors. For instance, the currently used f-value for λ1085 is underestimated by a factor of ∼38, while that for λ1031 is overestimated by a factor of ∼7. While the aim of this work is not to determine empirically the Cl I f-values in the *FUSE* bandpass, the set of revised f-values we present in Table 8 should provide a better match to the observations and can be used in the future for comparison with new theoretical calculations. For a comprehensive study of the oscillator strengths of many Cl I transitions, including several not covered here, we direct the reader to the work by Sonnentrucker et al. (2006).

Taking into account the uncertainties in the f-value of 1088, as well as on the measured equivalent width, and assuming that this transition in on the linear COG, we derive $\log N({\rm Cl\ I}) = 13.72 \pm 0.04$.

There is a weak absorption feature around 976 Å ($W_\lambda = 19.5 \pm 1.6$ Å), which we suspect to be from chlorine, as we have not been able to identify it with other lines of other atomic or molecular species. We use the H_2 ($J = 2$) λ975.3507 and HD ($J = 0$) λ975.5821 lines to derive the wavelength of this unknown transition by assuming that it traces the same absorption component as H_2 and HD. The *FUSE* wavelength solution is expected to be accurate to about 6 km s^{-1}, which at these wavelengths translates into ∼0.02 Å. We derive then $\lambda = 976.17$ Å for this unknown transition.

8. SUMMARY

We have used *FUSE* data to determine the abundance of several atomic and molecular species along the sight lines to HD 41161 and HD 53975. Together with N(H I) from the literature, we derive D/H, N/H, O/H, and D/O ratios for these sight lines. We find that while the D/H ratio along the HD 53975 sight line is consistent with five previous measurements at similar N(H), the ratio toward HD 41161 is surprisingly high and presents the first evidence of D/H variations for sight lines with high N(H). The pattern of low D/H for sight lines with large N(H), pointed out by Hébrard & Moos (2003) and emphasized by Wood et al. (2004) and Hébrard et al. (2005), is based on a small number of sight lines. Taking into account that at this high N(H) there is a selection bias against high D/H measurements (Oliveira et al. 2006), it is not surprising that only 1 out of 7 sight lines present high D/H ratios. As analyses of D/H along other high column density sight lines are being performed, one might expect that future measurements will also produce high D/H ratios, indicating that our understanding of the mechanisms responsible for the observed D/H pattern are still incomplete. Finally, the large number of Cl I transitions detected in the spectra of HD 41161 allows us to place significant constraints on the f-values of several transitions for which only theoretical values are available.

This work is based on data obtained for the Guaranteed Time Team by the NASA-CNES-CSA *FUSE* mission operated by the Johns Hopkins University. Financial support to US participants has been provided in part by NASA contract NAS5-32985 to Johns Hopkins University. Financial support to G. Hébrard has been provided by CNES. Based on observations made with the *International Ultraviolet Explorer*, obtained from the data archive at the Space Telescope Science Institute, which is operated by the Association of Universities for Research in Astronomy, Inc., under NASA contract NAS5-26555. Support for MAST for non-*HST* data is provided by the NASA Office of Space Science via grant NAG5-7584 and by other grants and contracts. The profile-fitting procedure, Owens.f, used in this work was developed by M. Lemoine and the French *FUSE* Team.

REFERENCES

Abgrall, H., Roueff, E., Launay, F., Roncin, J. Y., & Subtil, J. L. 1993a, A&AS, 101, 273
———. 1993b, A&AS, 101, 323
Allen, M. M., Jenkins, E. B., & Snow, T. P. 1992, ApJS, 83, 261
André, M. K., et al. 2003, ApJ, 591, 1000
Asplund, M., Grevesse, N., & Sauval, A. J. 2005, in ASP Conf. Ser. 336, Cosmic Abundances as Records of Stellar Evolution and Nucleosynthesis, ed. T. G. Barnes III & F. N. Bash (San Francisco: ASP), 25
Biemont, E., Gebarowski, R., & Zeippen, C. J. 1994, A&A, 287, 290
Bohlin, R. C., Savage, B. D., & Drake, J. F. 1978, ApJ, 224, 132
Cartledge, S. I. B., Lauroesch, J. T., Meyer, D. M., & Sofia, U. J. 2004, ApJ, 613, 1037
Conti, P. S., & Alschuler, W. R. 1971, ApJ, 170, 325
Diplas, A., & Savage, B. D. 1994a, ApJS, 93, 211
———. 1994b, ApJ, 427, 274
Dixon, W. V. D., Hurwitz, M., & Bowyer, S. 1998, ApJ, 492, 569
Draine, B. T. 2004, BAAS, 36, 1436
———. 2006, in ASP Conf. Ser. 348, Astrophysics in the Far Ultraviolet: Five Years of Discovery with *FUSE*, ed. G. Sonneborn, H. W. Moos, & B.-G. Andersson (San Francisco: ASP), 58
Epstein, R. I., Lattimer, J. M., & Schramm, D. N. 1976, Nature, 263, 198
Friedman, S. D., Hébrard, G., Tripp, T. M., Chayer, P., & Sembach, K. R. 2006, ApJ, 638, 847
Friedman, S. D., et al. 2002, ApJS, 140, 37
Garmany, C. D., Conti, P. S., & Massey, P. 1980, ApJ, 242, 1063
Gies, D. R., Fullerton, A. W., Bolton, C. T., Bagnuolo, W. G., Jr., Hahula, M. E., & Wiemker, R. 1994, ApJ, 422, 823
Hébrard, G. 2006, in ASP Conf. Ser. 348, Astrophysics in the Far Ultraviolet: Five Years of Discovery with *FUSE*, ed. G. Sonneborn, H. W. Moos, & B.-G. Andersson (San Francisco: ASP), 47
Hébrard, G., & Moos, H. W. 2003, ApJ, 599, 297
Hébrard, G., Tripp, T. M., Chayer, P., Friedman, S. D., Dupuis, J., Sonnentrucker, P., Williger, G. M., & Moos, H. W. 2005, ApJ, 635, 1136
Hébrard, G., et al. 2002, ApJS, 140, 103
Hoopes, C. G., Sembach, K. R., Hébrard, G., Moos, H. W., & Knauth, D. C. 2003, ApJ, 586, 1094
Howarth, I. D., Siebert, K. W., Hussain, G. A. J., & Prinja, R. K. 1997, MNRAS, 284, 265
Humphreys, R. M. 1978, ApJS, 38, 309
Jenkins, E. B. 1978, ApJ, 219, 845
———. 1986, ApJ, 304, 739
Jenkins, E. B., Tripp, T. M., Woźniak, P., Sofia, U. J., & Sonneborn, G. 1999, ApJ, 520, 182
Jura, M. 1974, ApJ, 190, L33
———. 1982, in Advances in Ultraviolet Astronomy: Four Years of *IUE* Research, ed. Y. Kondo, J. M. Mead, & R. D. Chapman (Washington, DC: NASA), 54
Jura, M., & York, D. G. 1978, ApJ, 219, 861
Kirkman, D., Tytler, D., Suzuki, N., O'Meara, J. M., & Lubin, D. 2003, ApJS, 149, 1
Kurucz, R. L., & Peytremann, E. 1975, SAO Special Report, 362
Lemoine, M., et al. 1999, NewA, 4, 231
———. 2002, ApJS, 140, 67
Linsky, J. L., Diplas, A., Wood, B. E., Brown, A., Ayres, T. R., & Savage, B. D. 1995, ApJ, 451, 335
Linsky, J. L., et al. 2006, ApJ, 647, 1106
Maíz-Apellániz, J., Walborn, N. R., Galué, H. Á., & Wei, L. H. 2004, ApJS, 151, 103
Meyer, D. M., Cardelli, J. A., & Sofia, U. J. 1997, ApJ, 490, L103
Meyer, D. M., Jura, M., & Cardelli, J. A. 1998, ApJ, 493, 222
Moos, H. W., et al. 2000, ApJ, 538, L1
Morton, D. C. 1991, ApJS, 77, 119
———. 2003, ApJS, 149, 205
Mullan, D. J., & Linsky, J. L. 1999, ApJ, 511, 502
Oliveira, C. M., Dupuis, J., Chayer, P., & Moos, H. W. 2005, ApJ, 625, 232
Oliveira, C. M., Hébrard, G., Howk, J. C., Kruk, J. W., Chayer, P., & Moos, H. W. 2003, ApJ, 587, 235
Oliveira, C. M., Moos, H. W., Chayer, P., & Kruk, J. W. 2006, ApJ, 642, 283
Prochaska, J. X., Tripp, T. M., & Howk, J. C. 2005, ApJ, 620, L39
Prodanović, T., & Fields, B. D. 2003, ApJ, 597, 48
Rachford, B. L., et al. 2002, ApJ, 577, 221
Rogerson, J. B., & York, D. G. 1973, ApJ, 186, L95
Romano, D., Tosi, M., Chiappini, C., & Matteucci, F. 2006, MNRAS, 369, 295
Sahnow, D. J., et al. 2000, ApJ, 538, L7
Savage, B. D., Bohlin, R. C., Drake, J. F., & Budich, W. 1977, ApJ, 216, 291
Schectman, R. M., Federman, S. R., Beideck, D. J., & Ellis, D. J. 1993, ApJ, 406, 735
Sembach, K. R., et al. 2004, ApJS, 150, 387
Sfeir, D. M., Lallement, R., Crifo, F., & Welsh, B. Y. 1999, A&A, 346, 785
Shull, J. M., & van Steenberg, M. 1982, ApJS, 48, 95
———. 1985, ApJ, 294, 599
Sonneborn, G., Tripp, T. M., Ferlet, R., Jenkins, E. B., Sofia, U. J., Vidal-Madjar, A., & Woźniak, P. R. 2000, ApJ, 545, 277
Sonnentrucker, P., Friedman, S. D., & York, D. G. 2006, preprint (astro-ph/0609132)
Spergel, D. N., et al. 2006, ApJ, submitted (astro-ph/0603449)
Williger, G. M., Oliveira, C., Hébrard, G., Dupuis, J., Dreizler, S., & Moos, H. W. 2005, ApJ, 625, 210
Wood, B. E., Linsky, J. L., Hébrard, G., Williger, G. M., Moos, H. W., & Blair, W. P. 2004, ApJ, 609, 838
York, D. G. 1983, ApJ, 264, 172